# cmgh

ORIGINAL RESEARCH

ZEB1 Transcriptionally Activates PHGDH to Facilitate Carcinogenesis and Progression of HCC

Huihui Wang,[1] Furong Lin,[1] Zhenzhen Xu,[1] Shengnan Yu,[2] Guannan Li,[1] Shan Liao,[3] Wentao Zhao,[1] Fengqiong Zhang,[1] Jinyang Wang,[1] Shijie Wang,[4] Cong Ouyang,[1] Cixiong Zhang,[1] Hailong Xia,[1] Yufei Wu,[5] Bin Jiang,[1] and Qinxi Li[1]

[1]The State Key Laboratory of Cellular Stress Biology, School of Life Sciences, Faculty of Medicine and Life Sciences, Xiamen University, Xiamen, China; [2]Organ Transplantation Institute of Xiamen University, Xiamen Key Laboratory of Regeneration Medicine, Fujian Provincial Key Laboratory of Organ and Tissue Regeneration, School of Medicine, Xiamen University, Xiamen, China; [3]First Department of Breast and Thyroid Surgery, Liuzhou People's Hospital, Liuzhou, Guangxi, China; [4]Department of General Surgery, Jinling Hospital, Medical School of Nanjing University, Nanjing, China; and [5]Department of Gynecology and Obstetrics, Zhongshan Hospital of Xiamen University, Xiamen, China
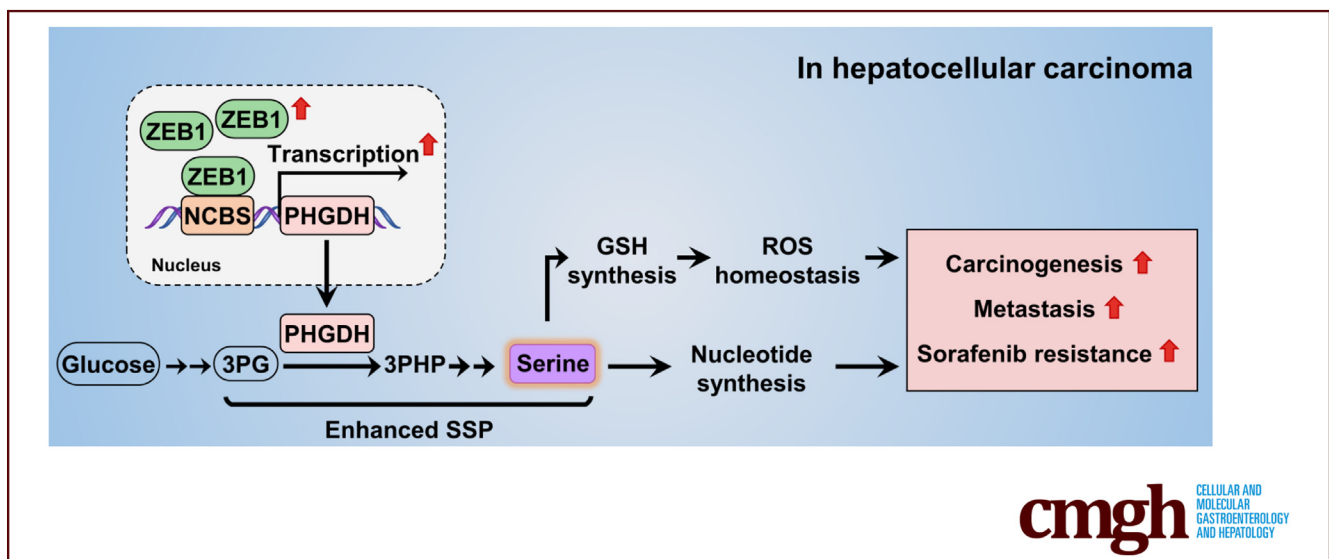
SUMMARY

Zinc finger E-box binding homeobox 1 reprograms the de novo serine synthesis pathway by transcriptionally activating phosphoglycerate dehydrogenase to stimulate carcinogenesis and metastasis of hepatocellular carcinoma, suggesting that the disruption of zinc finger E-box binding homeobox 1 transcriptional activity toward phosphoglycerate dehydrogenase is a potential strategy for the treatment of hepatocellular carcinoma.

BACKGROUND & AIMS: Phosphoglycerate dehydrogenase (PHGDH), the rate-limiting enzyme of the de novo serine synthesis pathway (SSP), has been implicated in the carcinogenesis and metastasis of hepatocellular carcinoma (HCC) because of its excessive expression and promotion of SSP. In previous experiments we found that SSP flux was diminished by knockdown of zinc finger E-box binding homeobox 1 (ZEB1), a stimulator of HCC metastasis, but the underlying mechanism remains largely unknown. Here, we aimed to determine how

SSP flux is regulated by ZEB1 and the contribution of such regulation to carcinogenesis and progression of HCC.

METHODS: We used genetic mice with *Zeb1* knockout in liver specifically to determine whether *Zeb1* deficiency impacts HCC induced by the carcinogen diethylnitrosamine plus CCl_4. We explored the regulatory mechanism of ZEB1 in SSP flux using uniformly-labeled [^{13}C]-glucose tracing analyses, liquid chromatography–mass spectrometry, real-time quantitative polymerase chain reaction, luciferase report assay, and chromatin immunoprecipitation assay. We determined the contribution of the ZEB1–PHGDH regulatory axis to carcinogenesis and metastasis of HCC by cell counting assay, methyl thiazolyl tetrazolium (MTT) assay, scratch wound assay, Transwell assay, and soft agar assay in vitro, orthotopic xenograft, bioluminescence, and H&E assays in vivo. We investigated the clinical relevance of ZEB1 and PHGDH by analyzing publicly available data sets and 48 pairs of HCC clinical specimens.

RESULTS: We identified that ZEB1 activates PHGDH transcription by binding to a nonclassic binding site within its promoter region. Up-regulated PHGDH augments SSP flux to enable HCC

cells to be more invasive, proliferative, and resistant to reactive oxygen species and sorafenib. Orthotopic xenograft and bioluminescence assays have shown that ZEB1 deficiency significantly impairs the tumorigenesis and metastasis of HCC, and such impairments can be rescued to a large extent by exogenous expression of PHGDH. These results were confirmed by the observation that conditional knockout of ZEB1 in mouse liver dramatically impedes carcinogenesis and progression of HCC induced by diethylnitrosamine/CCl$_4$, as well as PHGDH expression. In addition, analysis of The Cancer Genome Atlas database and clinical HCC samples showed that the ZEB1–PHGDH regulatory axis predicts poor prognosis of HCC.

CONCLUSIONS: ZEB1 plays a crucial role in stimulating carcinogenesis and progression of HCC by activating PHGDH transcription and subsequent SSP flux, deepening our knowledge of ZEB1 as a transcriptional factor in fostering the development of HCC via reprogramming the metabolic pathway. *(Cell Mol Gastroenterol Hepatol 2023;16:541–556; https://doi.org/10.1016/j.jcmgh.2023.06.006)*

L iver cancer is ranked as the sixth most common malignancy and the third most common cause of cancer-related death worldwide.[1] Hepatocellular carcinoma (HCC) is the most common liver cancer, which comprises 75%–85% of primary liver cancer.[2] Because of its aggressive metastasis and the fact that HCC often is diagnosed at an advanced stage, HCC has become the second-most lethal tumor next to pancreatic cancer.[3] Although numerous efforts to improve diagnosis and therapy have been made, the prognosis of patients with HCC is still far from satisfactory, with a 5-year survival rate of approximately 18%.[4] The main event causing the poor prognosis is postoperative recurrence, which is approximately 70% within 5 years after surgery in advanced HCC patients.[5] Metastasis is the most fundamental biological characteristic and a major cause of treatment failure and cancer death.[6] Therefore, insight into the mechanisms of HCC metastasis is of great significance for improving the survival rate of HCC patients.

Zinc finger E-box-binding homeobox 1 (ZEB1), a member of the ZEBs family of transcription factors, is found to be tightly associated with the progression of a variety of human cancers, including liver cancer,[7] lung cancer,[8] and pancreatic cancer.[9] Moreover, it has been reported that high expression of ZEB1 in HCC is correlated with advanced TNM stage, intrahepatic metastasis, and frequent recurrence.[10] Ordinarily, ZEB1 interacts with paired CACCT(G) E-box-like promoter elements on its target genes, and it either down-regulates or up-regulates the target genes by recruiting different co-suppressors or co-activators through its regulatory domains. For instance, ZEB1 binds to the E-box located in the promoter of *CDH1* (the gene that encodes E-cadherin), and recruits the C-terminal binding protein transcriptional co-repressor, leading to repression of *CDH1* transcription and induction of epithelial–mesenchymal transition. Because of the pivotal role of the ZEB1

regulatory effect on E-cadherin and epithelial–mesenchymal transition, it is considered the major regulator of tumor invasion and metastasis. However, little is known about whether ZEB1 affects cell metabolism.

Serine is a critical node for the biosynthesis of many molecules directly or indirectly, such as nonessential amino acids glycine and cysteine, pyrimidine nucleotide bases, and glutathione (GSH).[11,12] The enhanced de novo serine synthesis pathway (SSP), an important biomarker of metabolic reprogramming, recently was shown to be crucial for many cancer cells' survival, including liver cancer.[13–15] Consistent with the extensive need for serine in cancer cells, phosphoglycerate dehydrogenase (PHGDH) has been reported to be up-regulated in various cancers,[16–18] including HCC cells,[19] which makes PHGDH a putative oncogene. Recent studies have reported that PHGDH is up-regulated by glyceraldehyde-3-phosphate dehydrogenase and the nuclear factor erythroid 2-related factor 2 SUMOylation–reactive oxygen species (ROS) axis, consequently accelerating SSP and HCC development.[19,20] Moreover, it has been reported that PHGDH defines a metabolic subtype of lung adenocarcinoma with a poor prognosis,[21] and is a critical driver of sorafenib resistance in HCC.[22] However, whether PHGDH can promote metastasis of HCC remains to be fully illustrated.

Here, we show that ZEB1 enhances SSP via transcriptionally activating PHGDH by binding to the nonclassic ZEB1 binding sequence on the promoter region of it, and thus aggravates HCC tumorigenesis and metastasis.

Results

ZEB1 Enhances the Serine Synthesis Pathway by Up-Regulating PHGDH in HCC

ZEB1 is well documented to promote the proliferation and metastasis in various primary tumors and transformed cells.[7–9] However, whether ZEB1 is involved in tumor progression in vivo is largely unknown. To investigate the oncogenicity of ZEB1 in vivo, we crossed *Zeb1^flox/flox* mice with albumin-Cre mice to generate liver-specific *Zeb1* knockout mice (*Zeb1^flox/flox*; Alb-Cre$^+$) and their wild-type littermate (*Zeb1^flox/flox*; Alb-Cre$^-$). We found that *Zeb1* deficiency impaired the initiation and development of HCC significantly, and the incidence of primary liver tumors

Most current article

induced by diethylnitrosamine (DEN)/CCl$_4$ was reduced from 90% to 10% (Figure 1*A* and *B*). In addition, expression of ZEB1 was increased significantly in DEN/CCl$_4$-induced tumors in *Zeb1*$^{flox/flox}$; Alb-Cre$^-$ mice (Figure 1*C*), which was consistent with the expression of ZEB1 in HCC tissues from

clinical patients (Figure 1*D*), indicating that ZEB1 functions pivotally in the carcinogenesis and development of HCC. We also detected the expression of ZEB2, the homolog of ZEB1, and failed to find any difference of ZEB2 expression between tumor tissues and normal tissues (Figure 1*C* and *D*),
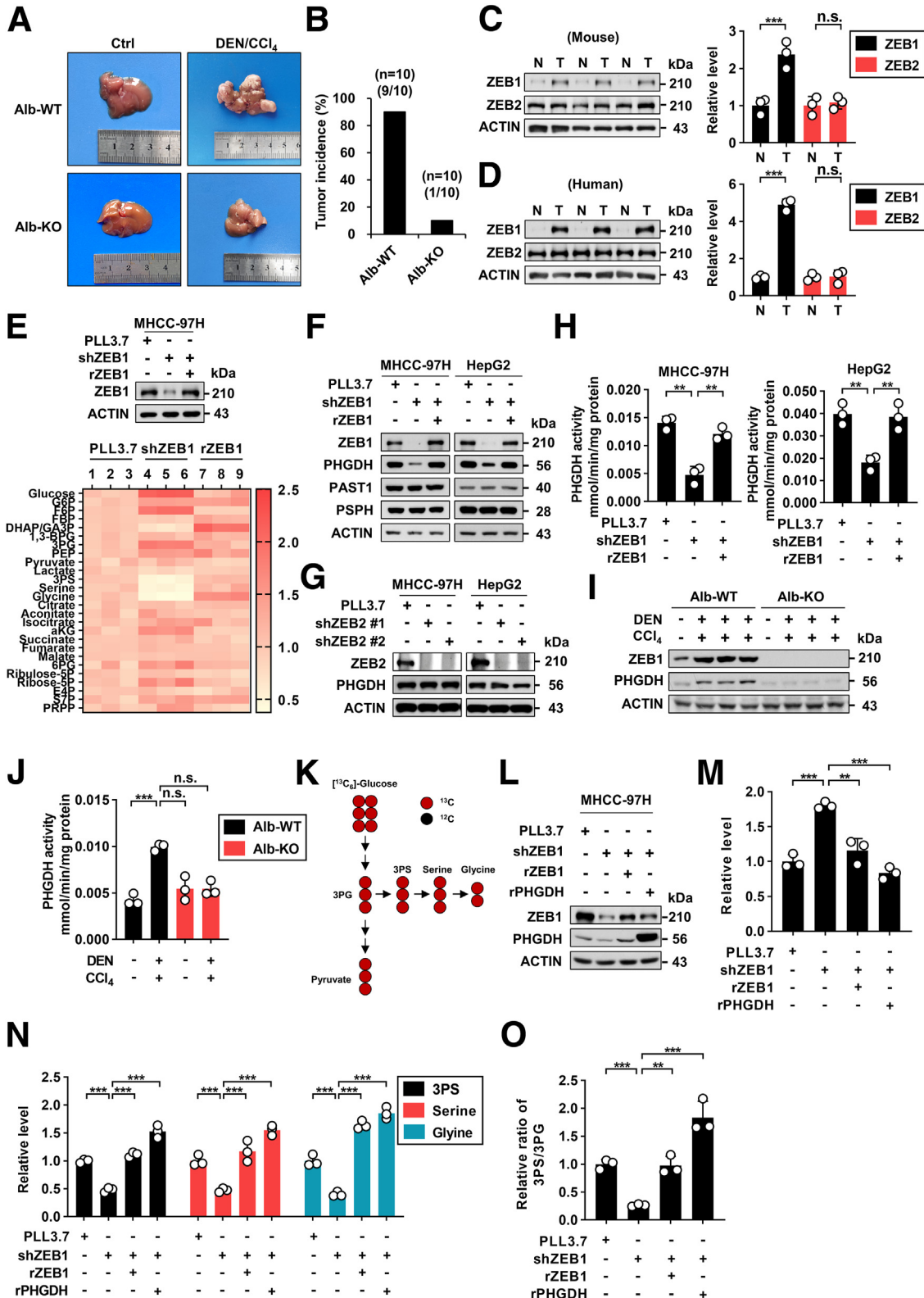
further showing the important role of ZEB1 in the tumorigenesis of HCC. To investigate whether ZEB1 is potentially associated with metabolic reprogramming in HCC, we knocked down ZEB1 in highly-metastatic hepatocellular carcinoma cell line-97 (MHCC-97H) cells and performed liquid chromatography–mass spectrometry (LC-MS) assays (Figure 1E). ZEB1 knockdown (KD) significantly diminished the abundance of metabolites in SSP, and re-expression of ZEB1 restored the SSP flux in ZEB1 KD cells (Figure 1E), suggesting that ZEB1 may promote HCC carcinogenesis by enhancing SSP flux.

To clarify how ZEB1 enhanced SSP flux, we detected the levels of enzymes in SSP, including PHGDH, phosphoserine aminotransferase, and phosphoserine phosphorylase in ZEB1 KD cells. Among the enzymes examined, PHGDH was exclusively decreased in ZEB1 KD cells, and re-expression of ZEB1 restored the PHGDH protein level (Figure 1F), showing that PHGDH expression is tightly regulated by ZEB1. Moreover, the expression of PHGDH was not altered by ZEB2 KD, further indicating that it is ZEB1 but not ZEB2 that regulates PHGDH expression (Figure 1G). To dissect the regulatory effect on PHGDH, we performed a PHGDH enzyme activity assay and found that the enzymatic activity of PHGDH decreased significantly in ZEB1 KD cell lines, and re-expression of ZEB1 restored the activity of PHGDH (Figure 1H), showing that ZEB1 enhances SSP by heightening the activity of PHGDH. Consistently, the proposal was confirmed by the observation that conditional knockout of ZEB1 in mouse liver dramatically impeded the expression and activity of PHGDH induced by DEN/CCl$_4$ (Figure 1I and J). To explore whether the ZEB1–PHGDH axis influenced cellular SSP flux, the metabolites of SSP were traced by uniformly-labeled [^{13}C]-glucose ([U-^{13}C]-glucose) (Figure 1K and L). An 80% increase in 3-phosphoglyceric acid concentration in ZEB1 KD cells was observed. In particular, re-expression of PHGDH completely reversed the accumulation (Figure 1M). Correspondingly, the abundance of SSP metabolites, including ^{13}C-labeled 3-phosphoserine, ^{13}C-labeled serine, and ^{13}C-labeled glycine, were decreased significantly in ZEB1 KD cells and could be restored by re-

expression of ZEB1 or PHGDH (Figure 1N). In addition, the ratio of 3-phosphoserine/3-phosphoglyceric acid decreased dramatically in ZEB1 KD cells, which largely reflected the activity of intracellular PHGDH (Figure 1O). Taken together, we suggest that ZEB1 enhances SSP by up-regulating PHGDH in HCC.

## ZEB1 Transcriptionally Activates PHGDH by Nonclassic Binding to its Promoter

Next, we explored how ZEB1 up-regulated the expression of PHGDH. Given that ZEB1 acted as a transcriptional factor, we examined the regulatory effect of ZEB1 on the PHGDH messenger RNA (mRNA) level. As expected, the mRNA level of PHGDH was diminished dramatically in ZEB1 KD cells and this decrease was completely rescued by re-expression of ZEB1, suggesting that ZEB1 may be a transcriptional activator of PHGDH (Figure 2A and B). To confirm this proposal, we cloned the -2093 to +87 base pair (bp) region of the PHGDH promoter into the pGL2 basic vector and performed a luciferase reporter assay (Figure 2C). PHGDH-Luciferase (PHGDH-Luc) was greatly activated by expression of ZEB1 in a dose-dependent manner (Figure 2D), which further indicates that PHGDH is transcriptionally activated by ZEB1. Then, we performed a chromatin immunoprecipitation assay and a real-time quantitative polymerase chain reaction (qPCR) assay to verify whether ZEB1 promoted PHGDH expression by directly binding to its promoter region. Indeed, DNA fragments of the PHGDH promoter region were enriched by immunoprecipitating ZEB1 as determined by PCR-based amplification and real-time qPCR (Figure 2E and F). In summary, ZEB1 activates the transcription of PHGDH by directly binding to the PHGDH promoter.

Previous studies have clarified that ZEB1 regulates the target genes by binding to E2-box-like element (CACCTG) located on the promoter regions.[23] To figure out whether ZEB1 bound to PHGDH promoter through the elements, we created various mutants with the elements mutated alone or in combination (Figure 2G). Surprisingly, the elements

Figure 1. (*See previous page*). **ZEB1 enhances the serine synthesis pathway by up-regulating PHGDH in HCC.** (*A*) Representative pictures of visualization of the primary liver tumor induced by DEN/CCl$_4$. (*B*) The incidence of tumor induced by DEN/CCl$_4$ was calculated. (*C*) Protein levels of ZEB1, ZEB2, and ACTIN in the tumor cohort induced by DEN/CCl$_4$ and the control cohort. (*D*) Protein levels of ZEB1, ZEB2, and ACTIN in HCC tissues and the corresponding adjacent normal tissues. (*E*) Metabolite change of the glucose-related pathway was analyzed by LC-MS and shown as a heatmap in MHCC-97H with ZEB1 KD and further re-expression of ZEB1. (*F*) Western blot analysis of the proteins involved in SSP with ZEB1 KD and further re-expression of ZEB1. (*G*) Western blot analysis of ZEB2, PHGDH, and ACTIN with ZEB2 KD. (*H*) Enzyme activity of PHGDH was determined in ZEB1 KD and further expressed for exogenous ZEB1 cells. (*I*) Western blot analysis of the protein levels in primary hepatocytes that were isolated from *Zeb1*$^{flox/flox}$; Alb-Cre$^-$ (Alb-WT) and *Zeb1*$^{flox/flox}$; Alb-Cre$^+$ (Alb-KO) mice induced by DEN/CCl$_4$ for 18 weeks. (*J*) Enzyme activity of PHGDH was determined in primary hepatocytes that were isolated from Alb-WT and Alb-KO mice. (*K*) The schematic diagram of the metabolic profiling showing [U-^{13}C]-glucose conversion to SSP. The red circles denotes uniformly ^{13}C-labeled positions of the carbons of glucose. (*L*) Western blot analysis of the ZEB1 and PHGDH protein levels in MHCC-97H cells prepared for LC-MS with ZEB1 KD and further re-expression of ZEB1 or PHGDH. (*M*) Relative abundance of ^{13}C-labeled 3-phosphoglyceric acid (3PG) was determined in the same MHCC-97H cell lines as in panel *L* using LC-MS. (*N*) The abundance of 3-phosphoserine (3PS), serine, and glycine derived from [U-^{13}C]-glucose in the same MHCC-97H cell lines as in panel *L* were measured using LC-MS. (*O*) The ratio of 3PS/3PG was calculated. The data are shown as means ± SD of 3 independent experiments and analyzed using the Student *t* test. **P < .01, ***P < .001, and n.s.: *P* ≥ .05. Ctrl, control; DHAP, dihydroxyacetone phosphate; E4P, erythrose 4-phosphate; FBP, fructose 1,6-bisphosphate; F6P, fructose 6-phosphate; GA3P, glyceraldehyde 3-phosphate; G6P, glucose 6-phosphate; N, normal; PEP, phosphoenolpyruvate; PRPP, phosphoribosyl pyrophosphate; rPHGDH, rescue PHGDH; rZEB1, rescue ZEB1; sh, short hairpin; S7P, sedoheptulose 7-phosphate; T, tumor; 3PS, 3-phosphoserine; 6PG, 6-phosphogluconic acid.

mutated in combination just slightly impaired the luciferase activity (Figure 2*H*), illustrating that the E2-box-like elements are not responsible for the activation of PHGDH by ZEB1. To find out the ZEB1 binding motif on the PHGDH promoter region, we constructed a series of truncated mutants of PHGDH promoter and measured their luciferase activity in the presence of ZEB1 (Figure 2*I*). We were surprised to find that region clone 3-b-1 and clone 3-b-2 (C3b-1 and C3b-2), which were truncated into 50 bp sequences (designated as the nonclassic binding site [NCBS]), retained
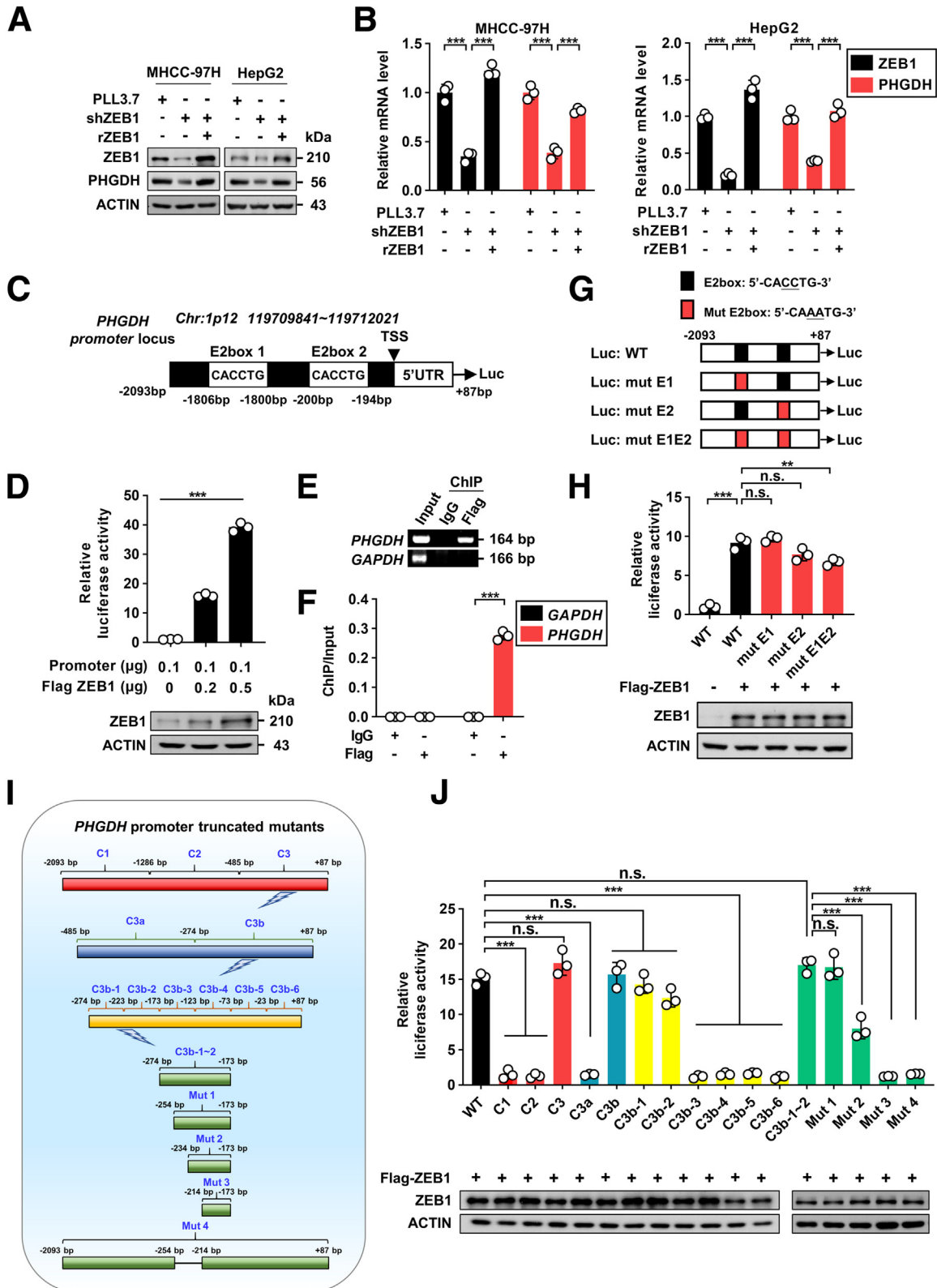
almost the whole luciferase activity of the full-length PHGDH promoter (Figure 2J). To further pinpoint the precise binding site of ZEB1 on the NCBS, we created deletion mutants (Mut 1–3) by sequentially deleting 20 bp each from the 5' end (Figure 2I). The luciferase results revealed a gradual decrease of Mut 1–3 in response to ZEB1. Consistent with this observation, Mut 4 deleted of -254 to -214 bp (a 40 bp sequence) lost the luciferase activity completely (Figure 2J), suggesting that the sequence containing these 40 bp is responsible for the activation of PHGDH transcription by ZEB1. Taken together, these results indicate that the NCBS sequence is either essential or sufficient for ZEB1 to activate the PHGDH transcription.

Activation of PHGDH by ZEB1 Promotes the Synthesis of GSH and Pyrimidine and Entrusts ROS and Sorafenib Resistance to HCC Cells

Because serine is the main provider of GSH and 1 carbon unit for pyrimidine (Figure 3A), we next explored PHGDH up-regulation by ZEB1 on the production of GSH and pyrimidine using [U-^{13}C]-glucose tracing. As expected, ZEB1 KD cells showed a decreased GSH level, and such decrease was rescued by ZEB1 or PHGDH overexpression (Figure 3B), indicating that activation of PHGDH by ZEB1 promotes the synthesis of GSH. It was reported that ROS served as a regulator of anoikis, which was a crucial barrier to tumor metastasis.[24,25] Considering the critical role of GSH as an antioxidant, we subsequently investigated whether such promotion of GSH synthesis contributed to intracellular ROS homeostasis, thereby enhancing the anoikis resistance of circulating tumor cells. Interestingly, we found that the levels of ROS were increased dramatically in ZEB1 KD cells, and re-expression of ZEB1 or PHGDH almost completely reversed the increased ROS levels (Figure 3C–E). It is particularly noteworthy that the addition of membrane-permeable GSH to ZEB1 KD cells not only effectively reduced ROS accumulation but also rescued the poor cellular state resulting from ZEB1 KD (Figure 3C–F). These findings provide compelling evidence that the ZEB1–PHGDH regulatory axis promotes HCC metastasis by enhancing GSH synthesis and resistance to anoikis. Next, we determined the contribution of the ZEB1–PHGDH regulatory axis to pyrimidine synthesis. ^{13}C-labeled deoxythymidine monophosphate (dTMP) was decreased significantly in ZEB1 KD cells, while natural deoxyuridine monophosphate (dUMP) had no alteration (Figure 3G and H), suggesting that up-regulation of PHGDH by ZEB1 may contribute to proliferation of HCC cells through enhancing pyrimidine synthesis. In view of studies indicating that up-regulation of PHGDH is the main cause of sorafenib resistance in HCC treatment, we detected the effect of the ZEB1–PHGDH regulatory axis on sorafenib resistance.[22,26] ZEB1 KD cells were more sensitive to sorafenib treatment than ZEB1 or PHGDH re-expressed cells (Figure 3I–K), showing that the ZEB1–PHGDH regulatory axis may be the main cause of sorafenib resistance. These data illustrate that the activated ZEB1–PHGDH regulatory axis promotes the synthesis of GSH and pyrimidine, and such promotion of GSH and pyrimidine synthesis may be a benefit to HCC tumorigenesis, metastasis, and resistance to ROS and sorafenib.

PHGDH Plays an Important Role in ZEB1-Stimulated Migration and Metastasis of HCC

We simultaneously aimed to know whether the ZEB1–PHGDH regulatory axis contributes to invasion and metastasis of HCC. In line with an earlier-described study, cell proliferation and cell viability were markedly impaired by ZEB1 KD, and further alleviated by replenishment of exogenous serine and re-expression of ZEB1 or PHGDH (Figure 4A–E), indicating that ZEB1 promotes cell proliferation at least partially via up-regulating PHGDH expression. We then explored whether the ZEB1–PHGDH regulatory axis functioned in HCC cell migration, invasion, and tumorigenesis. Consistently, the wound healing assay, Transwell assay, and soft-agar colony formation assay showed that ZEB1 KD remarkably weakened the migration, invasion, and tumorigenesis capabilities of HCC cells, and such weakening could be restored by re-expression of PHGDH (Figure 4F–H). These observations show that up-regulation of PHGDH by ZEB1 is crucial for HCC tumorigenesis, migration, and invasion.
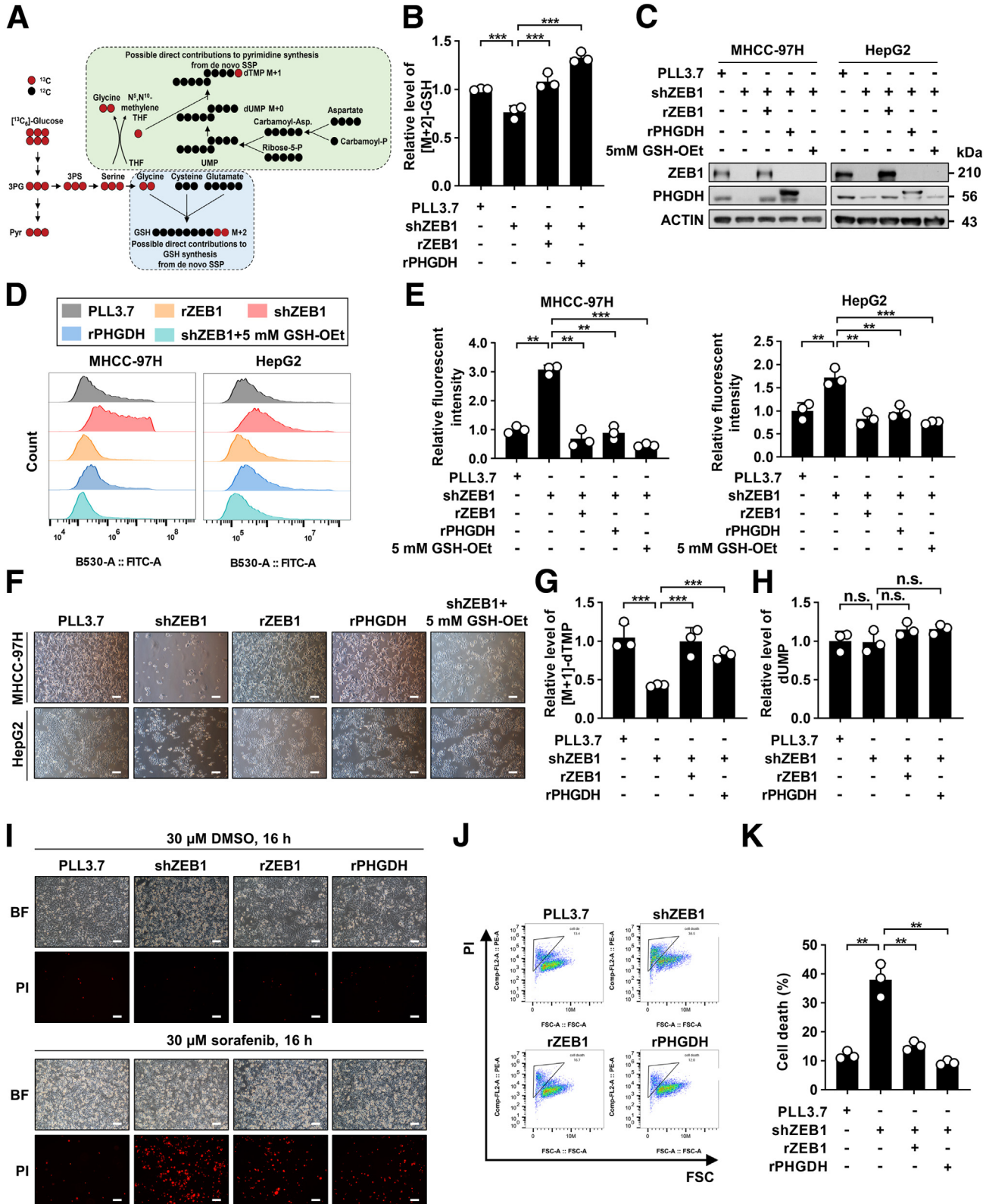
PHGDH Plays a Key Role in ZEB1-Stimulated Tumorigenesis and Metastasis of HCC In Vivo

To verify whether the ZEB–PHGDH regulatory axis accelerated HCC tumorigenesis and metastasis in vivo, we

---

Figure 2. (*See previous page*). ZEB1 transcriptionally activates PHGDH by nonclassic binding to its promoter. (*A*) Protein levels of cell lines that were prepared for real-time qPCR. (*B*) Relative mRNA levels of ZEB1 and PHGDH of cell lines in panel *A* were determined using real-time qPCR. (*C*) The schematic diagram of wild-type PHGDH promoter. (*D*) PHGDH-Luc and an increasing dose of ZEB1 were transfected into HEK-293T cells. Luciferase activity was determined after 24 hours of transfection. (*E*) Chromatin immunoprecipitation (ChIP) assay was performed in HEK-293T cells by using rabbit IgG and anti-Flag antibody. The glyceraldehyde-3-phosphate dehydrogenase (GAPDH) promoter served as a negative control. (*F*) The enrichment of PHGDH promoter in ChIP assay was determined by real-time qPCR. (*G*) Schematic diagram shows wild-type and E2-box mutant PHGDH promoters. (*H*) The corresponding luciferase activity of promoter mutants was determined by co-transfection with ZEB1 into HEK-293T cells. The relative luciferase activity was normalized to cells transfected only with wild-type PHGDH promoter (column 1). (*I*) Schematic diagram of wild-type PHGDH promoter and various truncated regions of PHGDH promoter. (*J*) The corresponding luciferase activity of various truncated regions of PHGDH promoter were determined by co-transfection with ZEB1 into HEK-293T cells. All luciferase activity was normalized to cells transfected with promoter alone. (*B, F, H,* and *J*) Data are shown as means ± SD of 3 independent experiments and analyzed using the Student *t* test. **$P < .01$, ***$P < .001$, and n.s.: $P \geq .05$. (*D*) Data are shown as means ± SD of 3 independent experiments and analyzed using 1-way analysis of variance. rZEB1, rescue ZEB1; sh, short hairpin.

performed a tumor formation experiment and biolumines-cence imaging assay (Figure 5A). Representative biolumi-nescence imaging (Figure 5B) showed that ZEB1 KD

impaired tumorigenesis and metastasis of HCC significantly, and mice of another 3 groups (LentiLox 3.7 [PLL3.7] group, rZEB1 group, and rPHGDH group) harbored more

metastatic nodules in colon and lung tissues (Figure 5C–F), further confirming the importance of the ZEB1–PHGDH regulatory axis in vivo. Moreover, the tumor size, tumor volume, and tumor weight of ZEB1 KD cell–derived xenografts were significantly smaller than that of xenografts derived from another 3 groups (Figure 5G–I), suggesting that ZEB1 aggravates the progression of HCC through increasing SSP by activating PHGDH. Summarily, these results show that PHGDH plays a key role in ZEB1-stimulated tumorigenesis and metastasis of HCC in vivo.

Interrelated High Expression of ZEB1 and PHGDH Is Correlated With Poor Prognosis of HCC

To confirm the importance of the ZEB1–PHGDH regulatory axis in the clinic, we analyzed The Cancer Genome Atlas Liver Hepatocellular Carcinoma database. RNA sequencing of patients at stage IV and tumor stage-4 (T4) showed a strong correlation between the mRNA levels of ZEB1 and that of PHGDH (Figure 6A). We then examined the expression of ZEB1 and PHGDH by staining successive tissue microarrays of HCC. Immunohistochemistry (IHC) staining results show that the expression of ZEB1 and PHGDH are markedly higher in tumor tissues than in corresponding adjacent normal tissues and showed highly positive correlation (Figure 6B–D), as well as in Western blot analysis (Figure 6E). Furthermore, data from Kaplan–Meier Plotter showed that in the ZEB1-high cohort, high expression of PHGDH was associated with a worse prognosis (Figure 6F). In conclusion, ZEB1 and PHGDH were up-regulated in HCC and their tight correlation predicted poor prognosis, reinforcing our proposal that ZEB1 promotes the progression of HCC at least partially by activating PHGDH transcription and resultant augmentation of SSP.

Discussion

Emerging evidence has shown that ZEB1 is tightly associated with many human cancers including HCC. The oncogenicity of ZEB1 is indicated by abnormal expression of ZEB1 in a wide array of human tumors and the fact that ZEB1 promotes proliferation and metastasis of varied primary and transformed cells.[27] However, little is known about whether ZEB1 promotes the progression of HCC in vivo. In this study,

we found that genetically depleted ZEB1 in mouse liver dramatically impeded primary HCC initiation. This observation provides convincing evidence that ZEB1 is indeed an oncogene that promotes HCC progression.

As a transcription factor, ZEB1 either down-regulates or up-regulates the downstream genes engaged in cell proliferation,[27] metabolism,[28] and cancer metastasis.[29] For instance, it is reported that ZEB1 activates integrin α3 transcription through yes-associated protein 1/transcriptional enhanced associate domain binding sites to impact the tumorigenesis and metastasis of pancreatic cancer.[30] In context of metabolism, ZEB1 is shown to transcriptionally activate phosphofructokinase-1,[31] glucose transporter 3,[32] and suppress fructose-1,6-bisphosphatase[33] to reprogram the metabolic pathway, which then promotes tumorigenesis of liver cancer and lung cancer. Here, our study establishes that ZEB1 transcriptionally up-regulates PHGDH to provide sufficient precursors for anabolic pathways, such as GSH and pyrimidine, indicating that the augmentation of anabolic pathways supports tumor cell proliferation in return.

In the multistep process of metastasis, tumor cells encounter a significant hurdle known as *anoikis*, which is triggered by the accumulation of ROS upon detachment from the extracellular matrix, leading to apoptosis.[24,25] Importantly, our study reveals that the ZEB1–PHGDH axis plays a crucial role in promoting GSH synthesis, which contributes to cellular ROS homeostasis and the survival of tumor cells. This suggests that ZEB1 may enhance the anoikis resistance of HCC cells, potentially through the activation of PHGDH and resultant augmentation of SSP, thus facilitating the metastasis of HCC.

Furthermore, the in situ HCC xenograft and bioluminescence assays show that the ZEB1–PHGDH regulatory axis functions importantly in the initiation and metastasis of primary liver tumor. Interestingly, we also found that silencing ZEB1 dramatically increased the sensitivity of MHCC-97H cells to sorafenib treatment. This effect may largely attribute to the diminishment of SSP flux and GSH synthesis because forced expression of PHGDH completely restored resistance to sorafenib in ZEB1 KD cells. In summary, we show that ZEB1 transcriptionally activates PHGDH to augment the SSP flux and facilitates the initiation and progression of HCC, broadening the role of ZEB1 in metabolism regulation.

Figure 3. (*See previous page*). **Activation of PHGDH by ZEB1 promotes the synthesis of GSH and pyrimidine and entrusts ROS and sorafenib resistance to HCC cells.** (*A*) Schematic diagram showing [U-^{13}C]-glucose conversion to GSH synthesis and pyrimidine synthesis contributed by SSP directly. The red circles denotes uniformly ^{13}C-labeled positions of the glucose carbons. (*B*) The abundance of ^{13}C-labeled GSH was determined in MHCC-97H ZEB1 KD cells with or without further expression of ZEB1 and PHGDH by LC-MS. (*C*) Western blot analysis of the cells prepared for ROS measurement. For ZEB1 KD cells that were supplied with exogenous glutathione monoethyl ester (GSH-OEt [sc-203974; Santa Cruz]), the cells were incubated with medium containing 5 mmol/L GSH-OEt for 48 hours. (*D*) Intracellular fluorescence of diacetato de 2′,7′-diclorofluoresceína (DCFH-DA) of the same cells in panel *C*. (*E*) Analysis of the intracellular fluorescent intensity of DCFHDA. (*F*) Representative pictures of cells with ZEB1 KD, re-expression of ZEB1 or PHGDH, and supplement of exogenous GSH-OEt. (*G*) The abundance of ^{13}C-labeled deoxythymidine monophosphate (dTMP) was determined in MHCC-97H ZEB1 KD cells with or without further expression of ZEB1 and PHGDH by LC-MS. (*H*) The abundance of natural deoxyuridine monophosphate (dUMP) was determined in MHCC-97H ZEB1 KD cells with or without further expression of ZEB1 and PHGDH by LC-MS. Cell death of cells that were treated with 30 μmol/L sorafenib was determined by (*I*) photographing and (*J*) flow cytometry. (*K*) Analysis of the cell death in panel *J*. (*F* and *I*) *Scale bars*: 200 μm. Data are presented as means $\pm$ SD of 3 independent experiments and analyzed using the Student *t* test. **P < .01, ***P < .001, and n.s.: *P* ≥ .05. BF, bright field; DMSO, dimethyl sulfoxide; FSC, forward scatter; PI, prodium iodide; Pyr, pyruvate; sh, short hairpin; THF, tetrahydrofuran; 3PG, 3-phosphoglyceric acid; 3PS, 3-phosphoserine.
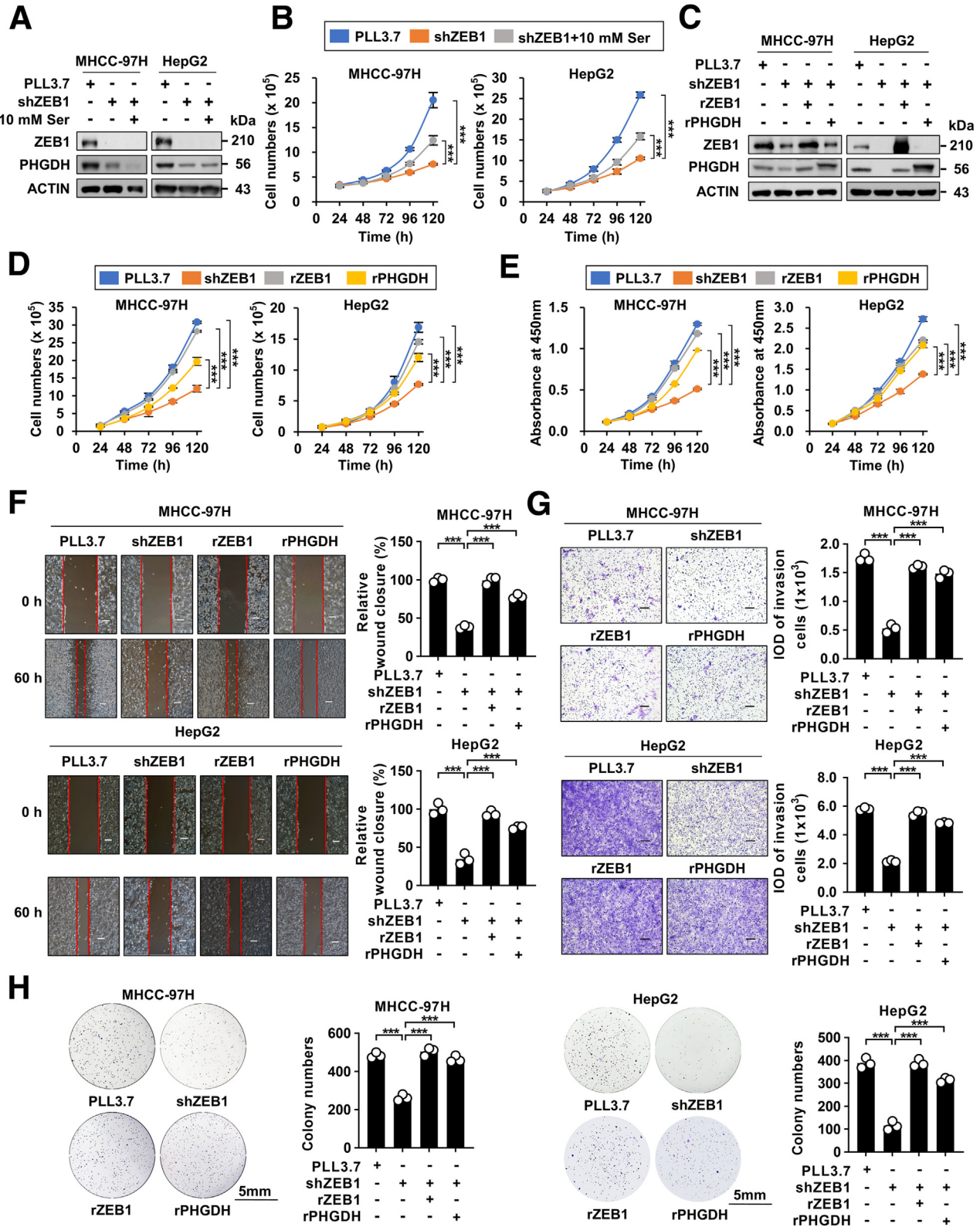
Figure 4. PHGDH plays an important role in ZEB1-stimulated migration and metastasis of HCC. (*A*) Western blot analysis of the cells prepared for cell proliferation assay in panel *B*. (*B*) ZEB1 KD cells were cultured in amino acid–free medium supplemented with 10 mmol/L serine or not, and cell proliferation was determined for the designated time using cell counting. (*C*) Western blot analysis of the cells prepared for assays in panels *D* and *E*. (*D*) Cell proliferation and (*E*) cell viability were determined using cell counting and the CCK-8 assay. Cell invasion, cell migration, and cell ability of tumorigenesis were determined using (*F*) wound healing assays, (*G*) Transwell assays, and (*H*) colony formation assays. *Scale bars*: 500 μm (*F* and *G*), 5 mm (*H*). The data are presented as means $\pm$ SD of 3 independent experiments and analyzed using the Student *t* test. ***$P < .001$, and n.s.: $P \geq .05$. IOD, integrated option density; rPHGDH, rescue PHGDH; rZEB1, rescue ZEB1; sh, short hairpin.
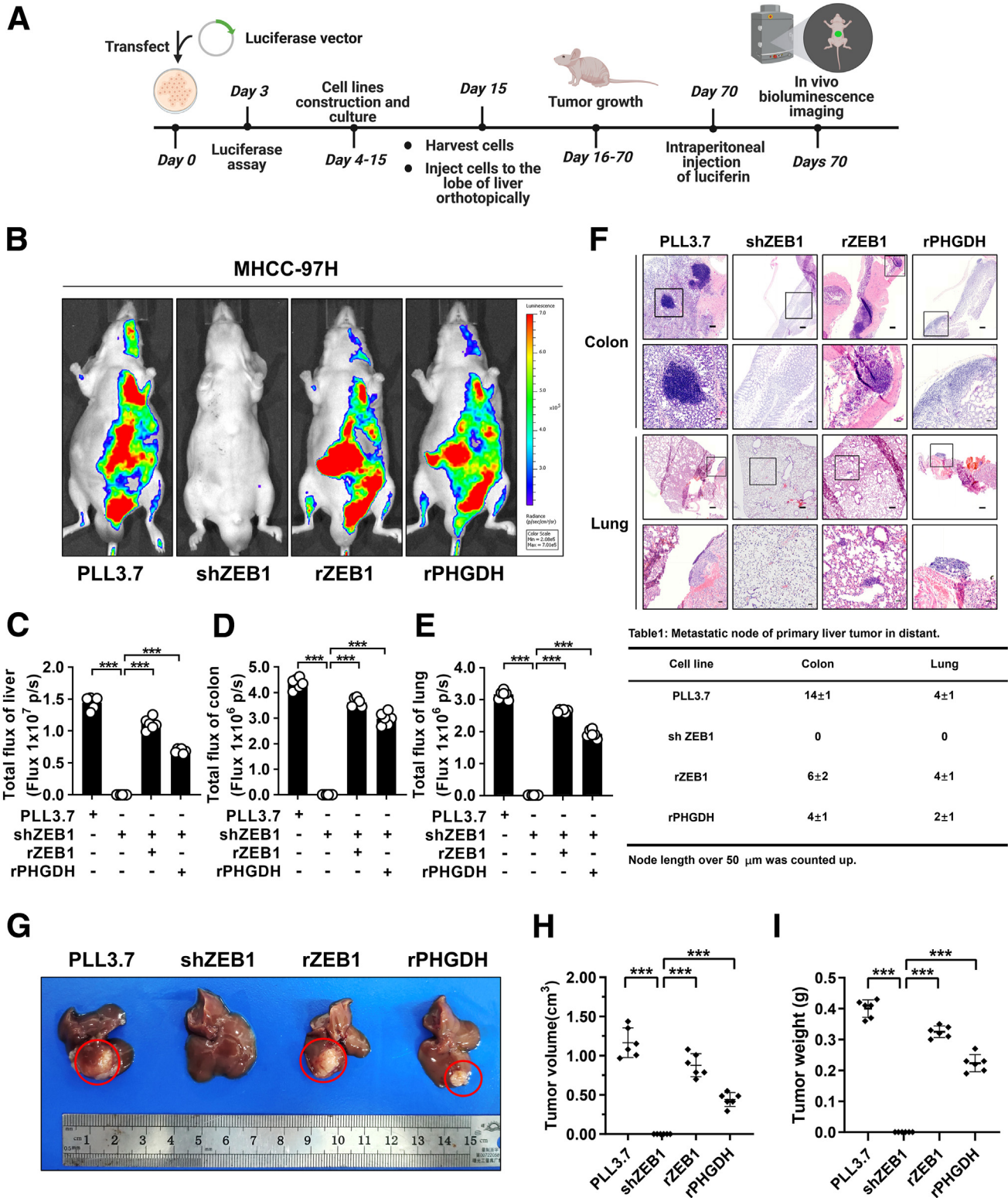
Figure 5. PHGDH plays a key role in ZEB1-stimulated tumorigenesis and metastasis of HCC in vivo. (*A*) Scheme for in vivo tracking of the ZEB1–PHGDH regulatory axis influence on HCC tumorigenesis and metastasis. (*B*) Representative images of visualization of the primary tumor in vivo after cellular orthotopic injection 8 weeks later, which was determined by bioluminescence imaging. Quantification of the bioluminescence imaging signals in (*C*) liver, (*D*) colon, and (*E*) lung. (*F*) Representative images of the liver, colon, and lung after H&E staining to determine the metastasis of the primary liver tumor. Metastasis node number was analyzed. *Scale bars*: 200 μm (*upper panel*), 50 μm (*lower panel*). (*G*) Representative pictures show mouse livers with tumor lesions (*red circles* indicate the primary tumor formed in the injection site). The (*H*) primary tumor volume and (*I*) primary tumor weight were determined. The data are presented as means $\pm$ SD of 6 mice and analyzed using the Student *t* test. ***$P <$ .001, and n.s.: $P \geq$ .05. Max, maximum; Min, minimum; rPHGDH, rescue PHGDH; rZEB1, rescue ZEB1; sh, short hairpin.
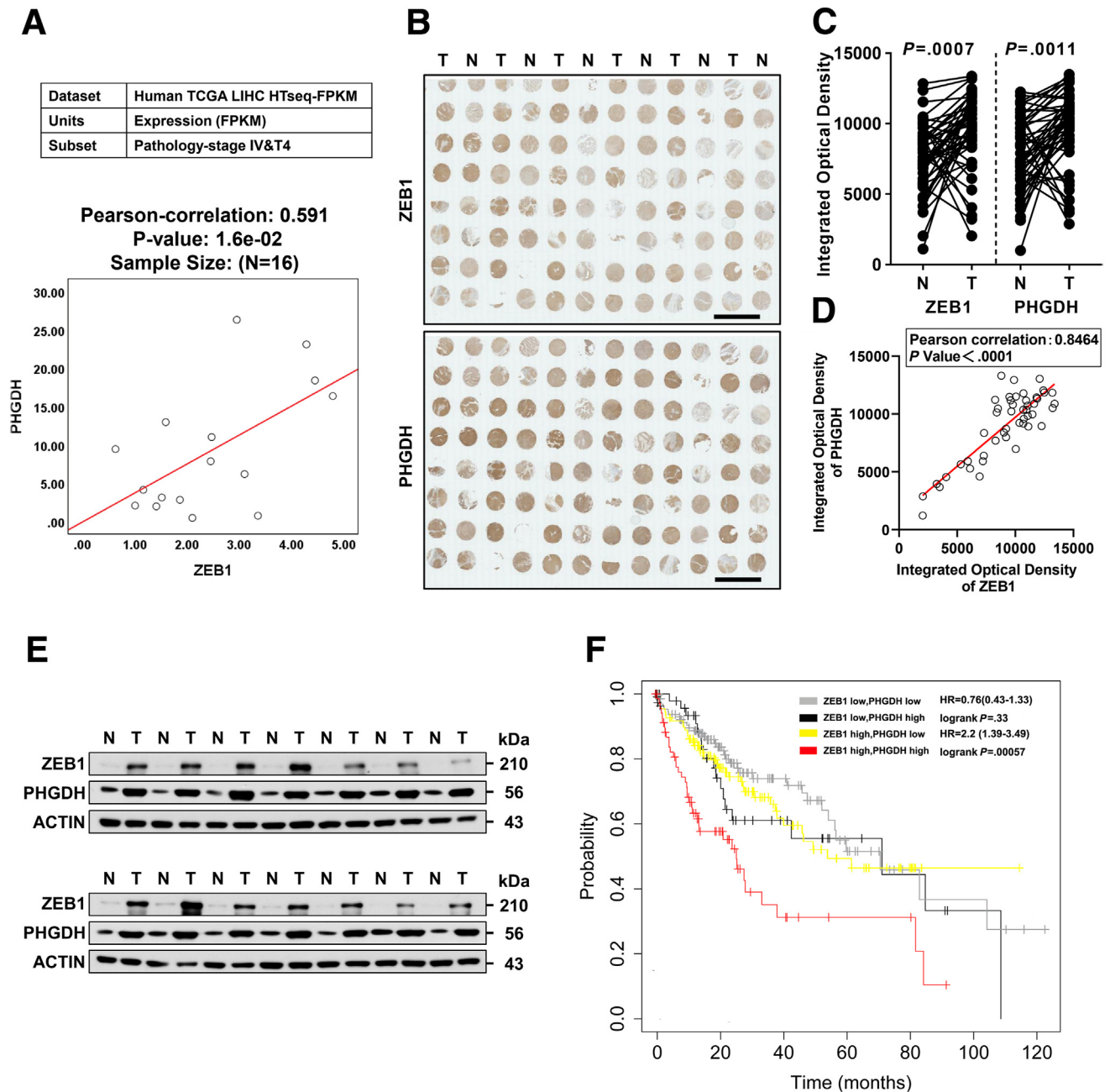
Figure 6. Interrelated high expression of ZEB1 and PHGDH is correlated with poor prognosis of HCC. (*A*) Correlation between ZEB1 and PHGDH of patients at stage IV and tumor stage-4 (T4) in The Cancer Genome Atlas (TCGA) Liver Hepatocellular Carcinoma (LIHC) database was analyzed by SPSS. IHC staining of successive HCC tissue microarrays (48 pairs) with (*B*) ZEB1 antibody and PHGDH antibody, and the (*C*) integrated optical density of ZEB1 and PHGDH in HCC tissues and the corresponding adjacent normal tissues were analyzed by ImageJ software, and (*D*) the correlation of ZEB1 and PHGDH in tumor cohort was analyzed by SPSS. (*B*) *Scale bars*: 4000 μm. (*E*) The protein levels of ZEB1 and PHGDH in HCC tissues and the corresponding adjacent normal tissues (N = 14) were determined using Western blot. (*F*) The Kaplan–Meier curves of overall survival basically relative to the ZEB1–PHGDH regulatory axis in HCC. Data are publicly available in the Kaplan–Meier Plotter. The data were analyzed by the Pearson chi-squared test. (*C*) Means $\pm$ SD are shown using the paired Student t test. FPKM, fragments per kilobase per million mapped reads; HR, hazard ratio; HTseq, high-throughput sequence analysis; N, normal; T, tumor.

Surprisingly, we uncover that inactive mutation of E2-box like elements on the PHGDH promoter region slightly impacts the regulatory effect of ZEB1 on PHGDH. To investigate the ZEB1 binding motif on the PHGDH promoter, we truncated the promoter region into different small regions and finally defined a nonclassic binding sequence that was indeed responsible for the regulation. This observation increased the complexity of

ZEB1 as a transcriptional factor in regulating different target genes.

Taken together, we explored the mechanism of ZEB1 in promoting HCC by activating the transcription of PHGDH in a nonclassic manner, establishing a direct link of ZEB1 to the promotion of SSP. Thus, disruption of the regulatory effect of ZEB1 on PHGDH may be a new strategy for the treatment of HCC and other cancers with excessive expression of PHGDH driven by ZEB1.

Materials and Methods
HCC Sample

This study was approved by the clinical research ethics committee of the First Affiliated Hospital of Xiamen University (Xiamen, Fujian, China). Before tissue acquisition, written informed consent was obtained from each patient according to the policies of the committee. Fourteen HCC tissues and paired nontumor tissues were used for Western blot analysis.

Animal Experiments

The experimental procedures were approved by the Institutional Animal Care and Use Committee at Xiamen University. For the xenograft tumor model, null mice (male, 5–6 weeks old) were purchased and housed in specific pathogen-free conditions. MHCC-97H cells (1×10^7) suspended in 50 μL phosphate-buffered saline (PBS) were injected into the same site of the left liver lobe of nude mice. Eight weeks after inoculation, D-luciferin was injected intraperitoneally at a concentration of 150 mg/kg and mice were anesthetized with pentobarbital. Ten minutes after injection, mice were imaged using an IVIS imaging system (Xenogen, Alameda, CA). Photons emitted from specific regions were quantified using Living Image software (Xenogen). In vivo luciferase activity was presented in photons emitted per second.

After being imaged, mice were killed. Livers were isolated, and the weight and size of the tumor were determined. Tumor volume was calculated as follows: tumor volume (cm^3) = (length [cm]) $\times$ (width [cm])^2 $\times$ 0.5. Then, livers, colons, and lungs were embedded into paraffin.

For the HCC tumor model induced by DEN-CCl$_4$, 2-week-old male mice in a C57BL/6 background were injected intraperitoneally with 2 mg/kg DEN (dissolved in PBS, body weight), then the mice were injected intraperitoneally with 5 mL/kg CCl$_4$ (20% dissolved in oil, body weight) twice a week for 12 weeks. Livers were isolated in the 20th week.

Plasmid Construction

Full-length human *ZEB1* and *PHGDH* were inserted into lentivirus vector pBoBi. Promoter fragments were cloned into pGL2 basic vector. LentiLox 3.7 (PLL3.7)-Neo-Green Fluorescent Protein (GFP) lentivirus vector was remolded into PLL3.7-Neo vector and then was used to express short hairpin RNA for knockdown. The synonymous point mutations residing in the short hairpin ZEB1 target sequence of Flag-tagged ZEB1 expression plasmid were created for RNA interference resistance. Luciferase was cloned into a PLV-puromycin vector for in vivo bioluminescent imaging. The primers are listed in Table 1.

Cell Culture and Stable Cell Line Construction

Cells were cultured in Dulbecco's modified Eagle medium (DMEM) supplemented with 10% fetal bovine serum (A24G00J; GEMINI) in a 37°C humid incubator containing 5% CO$_2$ and found to be negative for *Mycoplasma* infection using the PCR-based Mycoplasma Detection Kit (MP0035-1KT; Sigma). To obtain stable knockdown cells, lentiviral particles were generated by co-transfecting short hairpin RNA plasmid with packaging plasmid mix using the Hieff Trans Liposomal Transfection Reagent (40802ES03; YEA-SEN) in 293T cells and harvested 48 hours later, and cells then were infected with a proper amount of virus in the presence of polybrene (TR-1003-G; Merck Millipore) at a final concentration of 10 μg/mL. After 48 hours of infection, cells were selected with G418 (PP2374-1KT; Sigma) to obtain stable cell lines for the following experiments. A similar process was performed on the construction of cells re-expressing ZEB1 or PHGDH. To obtain stable luciferase-expressed cell lines for bioluminescent imaging, lentiviral particles of PLV-flag luciferase were generated and were added into MHCC-97H cells, and then the cells were treated with puromycin at a final concentration of 2 μg/mL for 72 hours. Next, MHCC-97H cells that expressed luciferase stably were infected with PLL3.7, Flag-ZEB1, and Flag-PHGDH lentiviral particles, respectively, and then MHCC-97H-Luc, MHCC-97H-Luc-Flag ZEB1, and MHCC-97H-Luc-Flag PHGDH were infected with short hairpin ZEB1 lentiviral particles.

Isolation of Primary Hepatocyte

Mice were anesthetized with pentobarbital (P3761; Sigma). Then, 20 mL perfusate (1 mmol/L ethylene glycol-bis(β-aminoethyl ether)-*N,N,N′,N′*-tetraacetic acid, 120 mmol/L NaCl, 50 mmol/L NaHCO$_3$, 5 mmol/L HEPES [pH 7.45], 5.55 mmol/L glucose, 4.8 mmol/L KCl, 2.5 mmol/L MgSO$_4$, and 1.2 mmol/L KH$_2$PO$_4$) was infused into the postcava of liver slowly, flowing out from the hepatic portal vein. Then, 20 mL digestion buffer (0.5 mg/mL collagenase II, 5 mmol/L CaCl$_2$, 120 mmol/L NaCl, 50 mmol/L NaHCO$_3$, 5 mmol/L HEPES [pH 7.45], 5.55 mmol/L glucose, 4.8 mmol/L KCl, 2.5 mmol/L MgSO$_4$, and 1.2 mmol/L KH$_2$PO$_4$) was infused. Subsequently, the liver was detached and the capsule was torn apart, and then cells were filtered by a 100-μm mesh. After being washed 3 times, cells were seeded into dishes.

Western Blot

Cells were harvested in a lysis buffer (20 mmol/L Tris-HCl [pH 7.4], 150 mmol/L NaCl, 1 mmol/L EDTA, 1 mmol/L ethylene glycol-bis(β-aminoethyl ether)-*N,N,N′,N′*-tetraacetic acid, 1% Triton X-100 (Sangon), 2.5 mmol/L sodium pyrophosphate, 1 mmol/L β-glycerophosphate, 1 mmol/L sodium orthovanadate, 1 mg/mL leupeptin, and 1 mmol/L phenylmethyl sulfonyl fluoride). The cell lysate was sonicated 5 times for 2 seconds each and then centrifuged at

Table 1. Primer Sequences Used

Gene	Forward primer 5' to 3'	Reverse primer 5' to 3'
Primers for overexpression		
ZEB1	ATGGCGGATGGCCCCAG	GGCTTCATTTGTCTTTTCTTC
PHGDH	ATGGCTTTTGCAAATCTGCGG	GAAGTGGAACTGGAAGGCTTC
Luciferase	ATGGAAGACGCCAAAAACATAAAG	CAATTTGGACTTTCCGCCCTTC
Primers for shRNA		
shZEB1	GGTAGATGGTAATGTAATA	
shZEB2#1	GGACACAGGTTCTGAAACA	
shZEB2#2	CTCAGAGTCCAATGCAGCACTTAGGTGTA	
Primers for re-expression of ZEB1		
rZEB1	GACGGAAATGTCATCAGGCAAGTGTTGGAGAATAA	GATGACATTTCCGTCAACCGCCACTTTAAGTACATT
Primers for real-time qPCR		
ZEB1	CGAACCCGCGGCGCAATA	CCAGCAGTTCTTAGCATTCC
PHGDH	AGGGAAATAACCAAAAAACTACCAAA	GCTACATGAACACAAAAACAGAGACC
ACTIN	TCCATCATGAAGTGTGACGT	TACTCCTGCTTGCTGATCCAC
Primers for ChIP		
PHGDH	GTCGAATTCCCTTCAACGTC	CCTGGTGAGCATATAAAAAGC
GAPDH	TACTAGCGGTTTTACGGGCG	TCGAACAGGAGGAGCAGAGAGCGA
Primers for luciferase plasmid		
Luc-WT	AATCGTGTCTCTGATTTAAGG	CGGCCGCTGTGAGTAGAAG
Luc-mut E1	ATAAAGAAAACAAATGATCAGGCTTAG	TGATCATTTGTTTTCTTTATTTATTATTT
Luc-mut E2	GCTCACCAAATGTAGGTAAGAGCTTTGG	ACCTACATTTGGTGAGCATATAAAA
Luc-C1	AATCGTGTCTCTGATTTAAGG	GTCCAACTAACCATTGTGTG
Luc-C2	TGGATATGTCCATAAAGCTG	GATGAGTTCATGTCCTTTGTAG
Luc-C3	ATTTTTTATGGCTGCATAGTATTC	CGGCCGCTGTGAGTAGAAG
Luc-C3a	ATTTTTTATGGCTGCATAGTATTC	CCTGAGAGAAAAACTTCATTT
Luc-C3b	ATGAGGTGTATTTCTCCGTTC	CGGCCGCTGTGAGTAGAAG
Luc-C3b ~ 1	ATGAGGTGTATTTCTCCGTTC	TACGCTGACTAGCTGATGC
Luc-C3b ~ 2	AATTGTGCTTTTTATATGC	CTCAGCCAAAGCTCTTACC
Luc-C3b ~ 3	ATGGAGAAATTCATCGCG	TTGCCAAATCCCTGCCCG
Luc-C3b ~ 4	CCTCAGAGCCGCGAGGAG	GGAAATACTCAAACTCTC
Luc-C3b ~ 5	GTCCAATCAAAAGGAGAC	GGAAATACTCAAACTCTC
Luc-C3b ~ 6	GAGCGGGAGCTGGAGAAT	CGGCCGCTGTGAGTAGAAG
Luc-C3b-1 ~ 2	ATGAGGTGTATTTCTCCGTTC	CTCAGCCAAAGCTCTTACC
Mut 1	CATTTCAGATATGCATCAGC	CTCAGCCAAAGCTCTTAC
Mut 2	TAGTCAGCGTAAATTGTG	CTCAGCCAAAGCTCTTAC
Mut 3	TTTATATGCTCACCAGG	CTCAGCCAAAGCTCTTAC
Mut 4	GTGTATTTCTCCGTTTTTATATGCTCACCAGG	AACGGAGAAATACACCTCATCCTGAGAGAAAAAC

ChIP, chromatin immunoprecipitation; C3b, clone 3-b; GAPDH, glyceraldehyde-3-phosphate dehydrogenase; shPHGDH, short hairpin PHGDH; shRNA, short hairpin RNA; shZEB, short hairpin ZEB; WT, wild-type.

12,500 rpm for 10 minutes at 4°C to obtain the supernatant. Proteins in total cell lysate were separated in 10% sodium dodecyl sulfate–polyacrylamide gel electrophoresis and transferred to a polyvinylidene difluoride membrane (Roche). The membrane was blocked with 5% nonfat milk in tris buffered saline with Tween 20 (TBST) buffer (20 mmol/L Tris-HCl, 150 mmol/L NaCl, and 0.1% Tween-20, pH 7.5) for 1 hour and incubated with corresponding antibodies. Proteins were visualized by enhanced chemiluminescence detection reagents. Antibodies are listed in Table 2.

LC-MS

MHCC-97H cells for LC-MS were cultured to approximately 80% confluence with medium containing 10 mmol/L [U-^{13}C]-glucose (110187-42-3; CIL) and 10% fetal bovine serum for 20 hours, then washed in precold PBS 3 times, quenched in 1 mL cold (-80°C) 80% methanol (methanol/water, v/v), and were detached from the culture dish using a cell scraper. Quenched cells were centrifuged at 12,000 × g for 15 minutes at 4°C, and 0.8 mL supernatant was dried by a vacuum freeze drier and dissolved in 100 μL aqueous–acetonitrile water. The mixture was centrifuged at 12,000 × g for 15 minutes and the supernatant was analyzed by LC-MS within 24 hours. Sample separation and analysis were performed on a Waters Acquity BEH C18 column (2.1 mm × 50 mm; particle size, 1.7 μm) using a gradient of buffer A (10 mmol/L tributylamine, 15 mmol/L acetic acid, 3% [v/v] methanol in water) and buffer B (methanol), using multiple reaction monitoring transitions.

PHGDH Enzyme Activity

Cells were seeded into 6-well plates to approximately 80% confluence, washed with precold PBS, and harvested by lysis buffer. Quenched cells were centrifuged at 12,000× g for 15 minutes at 4°C, and 10 μL supernatant was added to 96-well plates. Then premixed agent (333 mmol/L Tris/HCl [pH 9.0], 1.7 mmol/L EDTA [pH 9.0], 3.3 mmol/L

Table 2. Antibodies for Western Blot and IHC

Antibody	Source	Catalog number	Application (dilution)
ZEB1	Proteintech	21544-1-AP	WB (1:1000), IHC (1:200)
PHGDH	Proteintech	14719-1-AP	WB (1:1000), IHC (1:200)
PSAT1	Proteintech	10501-1-AP	WB (1:1000)
PSPH	Proteintech	14513-1-AP	WB (1:1000)
ZEB2	Proteintech	14026-1-AP	WB (1:1000)
IgG	Proteintech	14678-1-AP	ChIP (5 μg)
Flag	Proteintech	66008-4-Ig	ChIP (5 μg)
Actin	Proteintech	AC-15	WB (1:5000)

ChIP, chromatin immunoprecipitation; PSAT1, phosphoserine aminotransferase; PSPH, phosphoserine phosphorylase; WB, Western blot.

glutathione, 3 mmol/L oxidized nicotinamide adenine dinucleotide [NAD^+], 7 μg phosphoserine aminotransferase, 10 mmol/L glutamine, and 0.2 mmol/L 3-PG) was added to the corresponding wells, and the enzymatic activity determined by the production rate of reduced nicotinamide adenine dinucleotide (NADH) was measured by microplate reader at 340 nm. The enzymatic activity was normalized by protein concentration and calculated by the following equation: $\Delta OD340 * V/3.7715/ (\Delta t * m)$, where $\Delta OD340$, delta OD340; V, the total volume of enzyme activity assay (mL); Δt, delta time (min); and m, protein quality (mg).

Real-Time qPCR

Total RNA was extracted using TRIzol reagent (15596026; Invitrogen) according to the manufacturer's instructions. The first strand of complementary DNA was synthesized by the Revert Aid Reverse Transcriptase Kit (EP0441; Thermo Scientific) with oligo (deoxythymidine)$_{18}$ [oligo (dT)$_{18}$] primers. mRNA levels were normalized by β-actin and were determined using prevalidated SYBR Green Power Master Mix (4367659; Applied Biosystems). Amplification levels were detected using real-time PCR system (CFX384 Touch, Bio-Rad). All mRNA transcript levels were shown as the ratio of β-actin. The primers are listed in Table 1.

IHC Staining and H&E

Tissue sections and tissue microarray slides were deparaffinized by baking slides at 60°C for 3 hours. Then slides were rehydrated in a series of ethanol solutions. For IHC, slides were washed 3 times in PBS, then antigen retrieval was performed in boiling citrate-based solution for 20 minutes. After cooling down to room temperature, microarray slides were stained according to the manufacturer's instructions for the MaxVision DAB kit (KIT-0014; Maxim). For H&E, slides were stained with hematoxylin for 5 minutes, and 1% hydrochloric alcohol for 30 seconds. After being washed for 1 minute by aqua distillate, slides were stained by eosin for 3 minutes. Finally, the slides were sealed with neutral resin. The microarray slide images were captured using a Motic VM1 (1.0.8.21; Motic), and ImageJ

software (1.4.3.67; National Institutes of Health) was used to measure the sum of the integrated option density. The H&E-stained slices were photographed by a Panoramic digital Slide Microscan System (Leica Aperio Versa 200).

Luciferase Reporter Assay

The PHGDH genomic fragment containing promoter region -2093 to +87 bp was amplified and cloned into the pGL2-basic vector. The reporter plasmids were co-transfected with Flag-ZEB1 into human embryonic kidney 293T (HEK-293T) cells. Twenty-four hours after transfection, the luciferase activity was determined by the Luciferase Assay Kit (11401ES76; YEASEN) and was normalized by protein concentration. The primers are listed in Table 1.

Chromatin Immunoprecipitation Assay

One 100-mm dish of 90% confluence HEK-293T cells was prepared, and then 9 μg Flag-ZEB1 was transfected into the HEK-293T cells. Eight hours later, the medium was changed. Twenty-four hours later, cells were cross-linked with precold (4°C) 1% formaldehyde for 15 minutes at room temperature. Then, a final concentration of 0.125 mol/L glycine was added and mixed for 5 minutes to terminate the cross-link. Cells were lysed in a lysis buffer (50 mmol/L Tris-HCl [pH 8.0], 0.5 mmol/L EDTA, 1% sodium dodecyl sulfate, and protease inhibitors) and sonicated to break chromatin into fragments with an average length of 300∼600 bp, followed by immunoprecipitation with anti-Flag antibody and purification of immunoprecipitated DNA fragments. PCR then was performed to determine whether ZEB1 could bind to these DNA fragments. The PCR samples were separated and stained by electrophoresis in 2% agarose gel containing ethidium bromide. Real-time qPCR also was used to determine the abundance of a coprecipitated gene fragment. The primers are listed in Table 1.

ROS Measurement

Cells were collected and incubated with 2 mmol/L ROS probe (Diacetato de 2′,7′-diclorofluoresceína [DCFH-DA])

(D6883; Sigma) at 37°C for 20 minutes. Then cells were washed 3 times with PBS and the fluorescent intensity was measured by flow cytometry and analyzed by FlowJo software (14.0.0.0; BD bioscience).

Cell Death Measurement

Cells were incubated with 10 μg/mL propidium iodide (P4170; Sigma) at 37°C for 20 minutes. Then, all cells were collected and washed 3 times with PBS, and the fluorescent intensity was analyzed by flow cytometry.

Cell Proliferation and Cell Viability

For cell proliferation, 1×10^5 cells were seeded into a 6-well plate and cultured in complete DMEM at 37°C with 5% CO_2 for the designated time. Then cells were counted by Count Star (IC 1000; ALIT). For the cell counting kit-8 (CCK-8) assay, 2×10^3 cells were seeded into a 96-well plate and cultured in complete DMEM at 37°C in a humid incubator containing 5% CO_2 for the designated time. Cell viability was determined using the CCK-8 kit (40203ES76; YEASEN) according to the manufacturer's instructions. For cell proliferation, 3 independent experiments of each group were performed. For CCK-8, all tests were performed 3 times in quadruplicate.

Wound Healing Assay

Cells were seeded into a 6-well plate and cultured to 90% confluence. Then, the cell monolayer was scratched gently with a 200 μL pipette tip, washed twice with PBS to remove detached cells, and the remaining cells were incubated in medium without fetal bovine serum. The scratch areas were photographed at 0 and 60 hours. Experiment of each group was performed in triplicate.

Cell Invasion Assay

Cells (2×10^5) were seeded into the upper Transwell chamber (polycarbonate filter with 8-μm pores, coated with 200 μg/mL Matrigel [356237; Corning]) containing 200 μL serum-free medium. The bottom chamber was supplemented with 800 μL complete medium as a chemoattractant. After a 48-hour incubation, noninvasive cells were removed by a cotton swab from the upper surface of the filters and invasive cells on the lower surface of the filters were fixed with 4% formaldehyde for 10 minutes, and then were stained with 0.5% crystal violet at room temperature for 30 minutes. After being washed with PBS 3 times for 5 minutes each time, the cells were photographed. Experiment of each group was completed in triplicate.

Soft Agar Colony Formation Assay

Complete DMEM (0.5 mL) containing 0.35% agar was poured into 12-well plates and acted as a bottom layer. After solidifying, a 0.7-mL middle layer medium containing 0.35% agar and 1000 cells was poured. Then, 200 μL DMEM was added to protect the top layer from drying. The plates were placed in the incubator and the medium was changed every 3 days for 20 days. The colonies were fixed with 4% paraformaldehyde and stained with 0.1% crystal violet

solution. Experiments of each group were completed for 3 times independently.

Statistical Analysis

Statistical analysis was performed using GraphPad Prism 8 software, and data were expressed as means ± SD or means ± SEM where necessary. To identify significant differences in the data, statistical analyses were performed with the 2-tailed unpaired Student t test, the 2-tailed paired Student t test, Pearson chi-squared test, and 1-way analysis of variance.

References

1. Rumgay H, Arnold M, Ferlay J, et al. Global burden of primary liver cancer in 2020 and predictions to 2040. J Hepatol 2022;77:1598–1606.
2. Balogh J, Victor D III, Asham EH, et al. Hepatocellular carcinoma: a review. J Hepatocell Carcinoma 2016;3:41.
3. Craig AJ, von Felden J, Garcia-Lezana T, et al. Tumour evolution in hepatocellular carcinoma. Nat Rev Gastroenterol Hepatol 2020;17:139–152.
4. Vogel A, Meyer T, Sapisochin G, et al. Hepatocellular carcinoma. Lancet 2022;400:1345–1362.
5. Forner A, Llovet JM, Bruix J. Hepatocellular carcinoma. Lancet 2012;379:1245–1255.
6. Lin YL, Li Y. Study on the hepatocellular carcinoma model with metastasis. Genes Dis 2020;7:336–350.
7. Wang Y, Bu F, Royer C, et al. ASPP2 controls epithelial plasticity and inhibits metastasis through β-catenin-dependent regulation of ZEB1. Nat Cell Biol 2014; 16:1092–1104.
8. Yang Y, Ahn Y-H, Chen Y, et al. ZEB1 sensitizes lung adenocarcinoma to metastasis suppression by PI3K antagonism. J Clin Invest 2014;124:2696–2708.
9. Aghdassi A, Sendler M, Guenther A, et al. Recruitment of histone deacetylases HDAC1 and HDAC2 by the transcriptional repressor ZEB1 downregulates E-cadherin expression in pancreatic cancer. Gut 2012; 61:439–448.
10. Zhou Y-M, Cao L, Li B, et al. Clinicopathological significance of ZEB1 protein in patients with hepatocellular carcinoma. Ann Surg Oncol 2012;19:1700–1706.
11. Nelson DL, Lehninger AL, Cox MM. Lehninger principles of biochemistry. Macmillan, 2008:891–920.
12. Locasale JW. Serine, glycine and one-carbon units: cancer metabolism in full circle. Nat Rev Cancer 2013;13:572–583.
13. Davis JL, Fallon HJ, Morris HP. Two enzymes of serine metabolism in rat liver and hepatomas. Cancer Res 1970; 30:2917–2920.
14. Snell K. Enzymes of serine metabolism in normal, developing and neoplastic rat tissues. Adv Enzyme Regul 1984;22:325–400.
15. Zogg CK. Phosphoglycerate dehydrogenase: potential therapeutic target and putative metabolic oncogene. J Oncol 2014;2014:524101.
16. Possemato R, Marks KM, Shaul YD, et al. Functional genomics reveal that the serine synthesis pathway is essential in breast cancer. Nature 2011;476:346–350.

17. DeNicola GM, Chen P-H, Mullarky E, et al. NRF2 regulates serine biosynthesis in non–small cell lung cancer. Nat Genet 2015;47:1475–1481.

18. Yoon S, Kim JG, Seo AN, et al. Clinical implication of serine metabolism-associated enzymes in colon cancer. Oncology 2015;89:351–359.

19. Liu S, Sun Y, Jiang M, et al. Glyceraldehyde-3-phosphate dehydrogenase promotes liver tumorigenesis by modulating phosphoglycerate dehydrogenase. Hepatology 2017;66:631–645.

20. Guo H, Xu J, Zheng Q, et al. NRF2 SUMOylation promotes de novo serine synthesis and maintains HCC tumorigenesis. Cancer Lett 2019;466:39–48.

21. Zhang B, Zheng A, Hydbring P, et al. PHGDH defines a metabolic subtype in lung adenocarcinomas with poor prognosis. Cell Rep 2017;19:2289–2303.

22. Wei L, Lee D, Law CT, et al. Genome-wide CRISPR/Cas9 library screening identified PHGDH as a critical driver for sorafenib resistance in HCC. Nat Commun 2019; 10:4681.

23. Vandewalle C, Van Roy F, Berx G. The role of the ZEB family of transcription factors in development and disease. Cell Mol Life Sci 2009;66:773–787.

24. Li AE, Ito H, Rovira II, et al. A role for reactive oxygen species in endothelial cell anoikis. Circ Res 1999; 85:304–310.

25. Simpson CD, Anyiwe K, Schimmer AD. Anoikis resistance and tumor metastasis. Cancer Lett 2008; 272:177–185.

26. Fornari F, Giovannini C, Piscaglia F, et al. Elucidating the molecular basis of sorafenib resistance in HCC: current findings and future directions. J Hepatocell Carcinoma 2021;8:741.

27. Caramel J, Ligier M, Puisieux AJ. Pleiotropic roles for ZEB1 in cancer. Cancer Res 2018;78:30–35.

28. Morandi A, Taddei ML, Chiarugi P, Giannoni E. Targeting the metabolic reprogramming that controls epithelial-to-mesenchymal transition in aggressive tumors. Front Oncol 2017;7:40.

29. Krebs AM, Mitschke J, Lasierra Losada M, et al. The EMT-activator Zeb1 is a key factor for cell plasticity and promotes metastasis in pancreatic cancer. Nat Cell Biol 2017;19:518–529.

30. Liu M, Zhang Y, Yang J, et al. Zinc-dependent regulation of ZEB1 and YAP1 coactivation promotes epithelial-mesenchymal transition plasticity and metastasis in pancreatic cancer. Gastroenterology 2021; 160:1771–1783. e1.

31. Zhou Y, Lin F, Wan T, et al. ZEB1 enhances Warburg effect to facilitate tumorigenesis and metastasis of HCC by transcriptionally activating PFKM. Theranostics 2021; 11:5926.

32. Masin M, Vazquez J, Rossi S, et al. GLUT3 is induced during epithelial-mesenchymal transition and promotes tumor cell proliferation in non-small cell lung cancer. Cancer Metab 2014;2:1–14.

33. Zhang J, Wang J, Xing H, et al. Down-regulation of FBP1 by ZEB1-mediated repression confers to growth and invasion in lung cancer cells. Mol Cell Biochem 2016; 411:331–340.

Correspondence
Address correspondence to: Qinxi Li, PhD or Bin Jiang, PhD, School of Life Sciences, Xiang'an Campus, Xiamen University, Xiang'an South Road 4221-120, Xiang'an District, Xiamen, Fujian Province, 361102 China. e-mail: liqinxi@xmu.edu.cn or jiangbin@xmu.edu.cn.

Data Availability
The data generated in this study are available upon request from the corresponding author.